Available online at www.sciencedirect.com
SCIENCE DIRECT®
C. R. Mecanique 332 (2004) 473–486
COMPTES RENDUS MECANIQUE

Microgravity and transfers/Process control

Thermocapillary convection in cylindrical liquid bridges and annuli

Bok-Cheol Sim [a], Abdelfattah Zebib [b]

[a] *Department of Mechanical Engineering, Hanyang University, Ansan, Kyunggi-Do 425-791, South Korea*
[b] *Department of Mechanical and Aerospace Engineering, Rutgers University, Piscataway, NJ 08855-8058, USA*

Available online 9 April 2004

Abstract

Thermocapillary convection in liquid bridges and open cylindrical annuli is investigated in two- and three-dimensional numerical studies. The nondeformable free surfaces are either flat or curved as determined by the fluid volume, V, and the Young–Laplace equation. Dynamic free-surface deformations are discussed only in the axisymmetric models. Convection is steady and axisymmetric at sufficiently low values of the Reynolds number, *Re*, with either nondeformable or deformable surfaces. For the parameter ranges considered, it is found that only steady convection is possible at any *Re* in strictly axisymmetric computations. Transition to oscillatory three-dimensional motions occurs as *Re* increases beyond a critical value dependent on the aspect ratio, the Prandtl number, *Pr*, and V. Good agreement with available experiments is achieved in all cases. ***To cite this article: B.-C. Sim, A. Zebib, C. R. Mecanique 332 (2004).***

Résumé

Convection thermocapillaire dans les ponts liquides en géométries cylindrique et annulaire. La convection thermocapillaire dans des ponts liquides et les domaines cylindriques annulaires ouverts est étudiée dans des configurations bi et tri-dimensionnelles. En modèle 3D, les surfaces libres indéformables sont soit planes, soit courbées, suivant l'effet du volume de fluide, V et l'équation de Young–Laplace. Les déformations dynamiques de surface libre sont discutées pour le modèle axisymétrique. La convection est stationnaire et symétrique à de faibles valeurs de *Re* avec une surface déformable ou non. Pour la gamme des paramètres considérée, les résultats n'ont pas révélé d'état oscillatoire axisymétrique dans le pont liquide tant avec des surfaces libres déformables ou indéformables. La transition au régime tridimensionnel oscillant se produit en augmentant *Re*, au delà d'une valeur critique élevée dépendante du rapport de forme, du nombre de Prandtl, *Pr* et de V. Un bon accord avec les valeurs expérimentales disponibles est bien démontré dans chacun des cas étudiés. ***Pour citer cet article : B.-C. Sim, A. Zebib, C. R. Mecanique 332 (2004).***

Keywords: Fluid mechanics; Oscillatory thermocapillary convection; Surface deformation; Liquid bridge; Open cylindrical annulus

Mots-clés : Mécanique des fluides ; Convection thermocapillaire oscillatoire ; Déformation de surface ; Pont liquide ; Cylindrique annulaire ouvert

E-mail addresses: sbcsim@naver.com (B.-C. Sim), zebib@jove.rutgers.edu (A. Zebib).

1631-0721/$ – see front matter
doi:10.1016/j.crme.2004.02.017

1. Introduction

Thermocapillary convection is a surface tension flow driven by a temperature gradient along an interface. The induced surface tension variations, and hence free surface shear stresses, generate fluid motion in the liquid pool. It is well known that thermocapillary convection is steady and axisymmetric when the temperature difference between two side walls of an open cylindrical cavity or two disks of a cylindrical liquid bridge is sufficiently small. At moderate and large Prandtl number Pr, the axisymmetric flow undergoes transition to oscillatory time-dependent, three-dimensional convection as the temperature difference increases beyond a critical value, ΔT_c. This transition is the main focus of the present review.

In order to obtain homogeneous solids from crystal growth melt [1], the influence of buoyancy and thermocapillary forces needs to be understood. On Earth, both forces cause convection in the melt. However, in a microgravity environment (microgravity is about $10^{-5}g_0$ in space experiments [2], where g_0 is the normal Earth gravity), thermocapillary forces dominate and can drive unsteady convection. Unsteady convection is responsible for striations which are bands of different concentrations in the crystal. Therefore, understanding transition to oscillatory flows is important to material processing in space.

The most popular methods for growing crystals are the Czochralski and floating zone [3] techniques. Thermocapillary effects in these two techniques were summarized by Schwabe [1]. Here we consider thermocapillary convection in a pair of relevant cylindrical geometries: a liquid bridge in a half-zone model of the float-zone crystal-growth process as shown in Fig. 1(a), and an open cylindrical annulus heated from the outside wall as shown in Fig. 1(b) constituting a model for the Czochralski crystal growth system. Thermocapillary convection with either undeformable flat or curved surfaces is investigated by two- and three-dimensional numerical simulations, and critical conditions for transition to oscillatory states are established. Dynamic free-surface deformations are discussed only in the axisymmetric numerical simulations.

2. Thermocapillary convection in liquid bridges

Numerous experimental, theoretical, and direct numerical studies of surface tension driven flows are available. Preisser, Schwabe and Scharmann [4] demonstrated experimentally the occurrence of oscillatory convection in a liquid bridge with $Pr = 8.9$. They observed waves travelling in the azimuthal direction and a unique wavenumber, m, of about 2 regardless of aspect ratio. Velten, Schwabe and Scharmann [5] found that buoyant forces could stabilize thermocapillary convection in a liquid bridge by comparing results heated from above with those from below, and observed the effect of aspect ratio on the critical Re and frequency. Carotenuto et al. [6] reported on standing waves with $m = 1$ in microgravity experiments. Secondary instabilities from pulsating to rotating waves and to $m = 2$ from $m = 1$ were experimentally reported by Monti, Savino and Lappa [7] and Muehlner et al. [8], respectively. Transition to a chaotic thermocapillary flow was observed by Schwabe and Frank [9]. Schwabe and Velten [10] reported restationarization above a critical Marangoni number in a long floating zone.

The influence of free surface shape as determined by the liquid volume was experimentally reported by Hu et al. [11], Masud, Kamotani and Ostrach [12], Shevtsova, Mojahed and Legros [13] and Sumner et al. [14]. It is evident from the experiments that two branches exist in a stability diagram ($\Delta T_c - V$). The critical wavenumber could be switched from 1 to 2 by changing the surrounding conditions and thus heat loss from the liquid bridge [13].

Smith and Davis [15] discussed the instability mechanisms of flows in an infinite liquid layer by linear stability theory. Linear instability of an infinite liquid bridge was investigated by Xu and Davis [16]. Kuhlmann and Rath [17] considered linear instability of steady axisymmetric thermocapillary flow in a liquid bridge with an aspect ratio of 1. They found that the most dangerous disturbance was either a pure hydrodynamic steady mode or an oscillatory hydrothermal wave, depending on Pr. Levenstam and Amberg [18] confirmed a first bifurcation from a steady axisymmetric flow to a steady nonaxisymmetric 3D flow at low Pr. Wanschura et al. [19] further investigated the primary instability of axisymmetric steady thermocapillary flow in a liquid bridge. They confirmed

the earlier results of Neitzel et al. [20], and provided a stability diagram for $Pr \leqslant 4.8$ with an aspect ratio of 1. Recently, a linear stability diagram for $Pr \leqslant 7$ was reported in detail by Levenstam, Amberg and Winkler [21]. Both stability boundaries are roughly in good agreement. The effect of liquid volume on instability in a liquid bridge was investigated by Chen and Hu [22]. However, their results of linear stability with a cylindrical surface and $Pr = 1$ were very different from those of other studies [19–21].

Tao, Sakidja and Kou [23] studied steady thermocapillary convection in a liquid bridge with a nondeformable curved surface by axisymmetric numerical simulations. Experimental and numerical studies on $Pr = 30$ and 74 oscillatory convection with a cylindrical surface were reported by Savino and Monti [24]. They observed pulsating and rotating waves with a wavenumber of 1. Shevtsova and Legros [25] investigated oscillatory convection in deformed liquid bridges with $Pr = 105$ by axisymmetric numerical simulations. While oscillatory buoyant-thermocapillary convection in the liquid bridge was reported with axisymmetric models, oscillatory thermocapillary convection with $Pr = 105$ was not found in the simulations [25]. The three-dimensional numerical simulations by Leypoldt, Kuhlmann and Rath [26] showed that standing waves evolved into travelling waves with $Pr = 4$ and 7. The influence of temperature-dependent viscosity was reported in a three-dimensional study by Shevtsova, Melnikow and Legros [27].

Three-dimensional numerical simulations with undeformable curved surfaces were first performed in a low *Pr* liquid bridge by Lappa, Savino and Monti [28]. They studied the transition to steady nonaxisymmetric state with $Pr = 0.01$. Oscillatory thermocapillary convection at moderate *Pr* was computed in an open cylinder and a liquid bridge with nondeformable curved surfaces by Sim and Zebib [29,30]. They showed that only steady thermocapillary convection with either flat or curved surfaces was possible in strictly axisymmetric computations, while oscillatory convection was three-dimensional.

2.1. Mathematical and numerical models

The physical system considered is a cylindrical liquid bridge with either flat or curved surface as shown in Fig. 1(a). The aspect ratio, *Ar*, is defined as R/H, where R and H are respectively the radius and height of the liquid bridge. The upper and lower disks have dimensionless temperatures $T_h = 1$ and $T_c = 0$, respectively. The surface tension is assumed a linear function of temperature,

$$\sigma = \sigma_o - \gamma(T - T_o) \tag{1}$$

where $\gamma = -\partial\sigma/\partial T$, and subscript o represents a reference state.

Neglecting body forces, the nondimensional governing equations are as follows:

$$\nabla \cdot \mathbf{v} = 0 \tag{2}$$

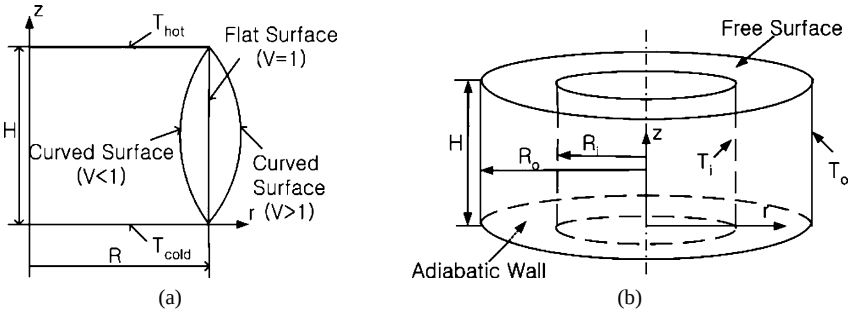

Fig. 1. Physical system: (a) a liquid bridge; (b) an open annulus.

Fig. 1. Système physique : (a) pont liquide ; (b) domaine annulaire ouvert.

$$Re\left(\frac{\partial \mathbf{v}}{\partial t} + \nabla \cdot (\mathbf{vv})\right) = -\nabla P + \nabla^2 \mathbf{v} \tag{3}$$

$$Ma\left(\frac{\partial T}{\partial t} + \nabla \cdot (\mathbf{v}T)\right) = \nabla^2 T \tag{4}$$

where $\mathbf{v}$ is the nondimensional velocity vector, and P and T are the nondimensional pressure and temperature. Re is the Reynolds number, Pr is the Prandtl number, and Ma is the Marangoni number defined by

$$Re = \gamma \frac{\Delta T H}{\nu \mu}, \qquad Pr = \frac{\nu}{\alpha}, \qquad Ma = Pr \cdot Re \tag{5}$$

where ν, μ, and α are kinematic viscosity, dynamic viscosity, and thermal diffusivity respectively. The length, temperature, velocity, pressure, and time are normalized with respect to H, ΔT, $\frac{\gamma \Delta T}{\mu}$, $\frac{\gamma \Delta T}{H}$, and $\frac{\mu H}{\gamma \Delta T}$, respectively. ΔT is the temperature difference between the upper and lower disks.

The velocities in the r, z, and θ directions of a cylindrical coordinate system are u, v, and w, respectively. The boundary conditions at the upper and lower walls become

$$u = 0, \quad v = 0, \quad w = 0, \quad T = 0, \quad \text{at } z = 0 \tag{6}$$

$$u = 0, \quad v = 0, \quad w = 0, \quad T = 1, \quad \text{at } z = 1 \tag{7}$$

2.1.1. Boundary conditions at the undeformable free surface

The nondimensionalized position of the free surface is described by a function $r = g(z)$. Thermal, kinematic and tangential stress balance boundary conditions at the interface are

$$-\frac{1}{N}\left(\frac{\partial T}{\partial r} - g'\frac{\partial T}{\partial z}\right) = Bi\, T \tag{8}$$

$$u = g' v \tag{9}$$

$$\left(1 - g'^2\right)\left(\frac{\partial v}{\partial r} + \frac{\partial u}{\partial z}\right) + 2g'\left(\frac{\partial u}{\partial r} - \frac{\partial v}{\partial z}\right) = -N\left(g'\frac{\partial T}{\partial r} + \frac{\partial T}{\partial z}\right) \tag{10}$$

$$\frac{\partial w}{\partial r} - \frac{w}{r} + \frac{1}{r}\frac{\partial u}{\partial \theta} - g'\left(\frac{\partial w}{\partial z} + \frac{1}{r}\frac{\partial v}{\partial \theta}\right) = \frac{-N}{r}\frac{\partial T}{\partial \theta} \tag{11}$$

where $N = (1 + g'^2)^{1/2}$ and $g' = \mathrm{d}g/\mathrm{d}z$. The Biot number in Eq. (8) is given by $Bi = hH/k$ where h is a heat transfer coefficient to the surroundings at the cold wall temperature, and k is the thermal conductivity of the liquid. The derivation of the boundary conditions and interface equation can be found in [31].

The location of the interface, $g(z)$, is determined by the normal stress balance. The deviation of the free surface shape from the static meniscus depends on the Capillary number, $Ca = \gamma \Delta T/\sigma_o$. When $Ca \ll 1$, dynamic surface deformations can be neglected [32], and the normal stress balance equation simplifies to the Young–Laplace equation. The interface and liquid volume equations in a state of rest are as follows:

$$-Ca \Delta P = \frac{1}{N}\left(\frac{g''}{N^2} - \frac{1}{g}\right) \tag{12}$$

$$V = \frac{1}{Ar^2}\int_0^1 g^2 \,\mathrm{d}z \tag{13}$$

where $\Delta P = P - P_o$ is the nondimensional pressure difference between the interface liquid and gas pressures, and the liquid volume is normalized with respect to $\pi R^2 H$. Eq. (12) has two boundary conditions, $g(0) = Ar$ and $g(1) = Ar$. The shape of the interface and ΔP are fixed with a prescribed liquid volume.

2.1.2. Boundary conditions at the deformable free surface in axisymmetric model

In reality, the free-surface profile, g, is unknown and should be obtained as a solution to the coupled transport equations along with surface force balances. The position of the free surface is described by a function $r = g(t, z)$. Thermal, kinematic and tangential and normal stress balance boundary conditions at the interface are

$$-\frac{1}{N}\left(\frac{\partial T}{\partial r} - g'\frac{\partial T}{\partial z}\right) = Bi\,T \tag{14}$$

$$u = \frac{\partial g}{\partial t} + g'v \tag{15}$$

$$\left(1 - g'^2\right)\left(\frac{\partial v}{\partial r} + \frac{\partial u}{\partial z}\right) + 2g'\left(\frac{\partial u}{\partial r} - \frac{\partial v}{\partial z}\right) = -N\left(g'\frac{\partial T}{\partial r} + \frac{\partial T}{\partial z}\right) \tag{16}$$

$$-P + \frac{2}{N^2}\left[\frac{\partial u}{\partial r} + g'^2\frac{\partial v}{\partial z} - g'\left(\frac{\partial v}{\partial r} + \frac{\partial u}{\partial z}\right)\right] = \frac{1 - CaT}{CaN}\left(\frac{g''}{N^2} - \frac{1}{g}\right) \tag{17}$$

where $g' = \partial g/\partial z$.

The tangential stress balance equation (16) defines the driving thermocapillary forces. The initial and boundary conditions for Eq. (17) considered here are:

$$\begin{aligned} &g(t = 0, z) = Ar \\ &g(t, z = 0) = Ar \\ &g(t, z = 1) = Ar \end{aligned} \tag{18}$$

The liquid volume must satisfy the mass conservation, and its total volume should be constant:

$$V = \frac{1}{Ar^2}\int_0^1 g^2\,\mathrm{d}z = 1 \tag{19}$$

where the liquid volume is normalized with respect to $\pi R^2 H$. Ca provides a measure of the surface deflection in response to thermocapillary-induced stresses. If $Ca = 0$ (large surface tension), the free surface is undeformable and flat.

In order to numerically solve the problem with either undeformable or deformable surfaces, the governing equations are transformed from the physical domain into a rectangular computational domain. The transformed equations and boundary conditions are solved by a finite volume method employing a SIMPLER algorithm. The transformed equations and numerical aspects can be found in [30] for undeformable surfaces and [33] for two-dimensional deformable surfaces.

2.2. Axisymmetric thermocapillary convection with either nondeformable or deformable interfaces

We have investigated thermocapillary convection up to $Re = 5000$ with $Pr = 1,\ Ar = 1,\ V = 1,\ Bi = 0$ and various Ca ($\leqslant 0.1$), and have found no oscillatory axisymmetric states in liquid bridges with either nondeformable or deformable free surfaces. Assuming nondeformable flat interfaces with $Pr = 1$ and $Ar = 1$, the critical Re for transition to oscillatory states is about 2500 from linear theory [19] and three-dimensional numerical simulations [30]. Since Ca is in the range $\mathrm{O}(10^{-2})$–$\mathrm{O}(10^{-3})$ in most experiments [34], we conclude that dynamic free-surface deformations do not induce transition to oscillatory, axisymmetric convection. Thus only azimuthal waves can generate oscillations in a liquid bridge with either nondeformable or deformable free surfaces. In addition, we have computed axisymmetric convection up to $Re = 1000$ with undeformable flat surfaces ($Pr = 27$, $Ar = 0.714$, $Bi = 0$), and no unsteady, oscillatory convection was found. The critical Re was 210 with a flat surface in three-dimensional numerical simulations. This is consistent with studies of convection in other cylindrical

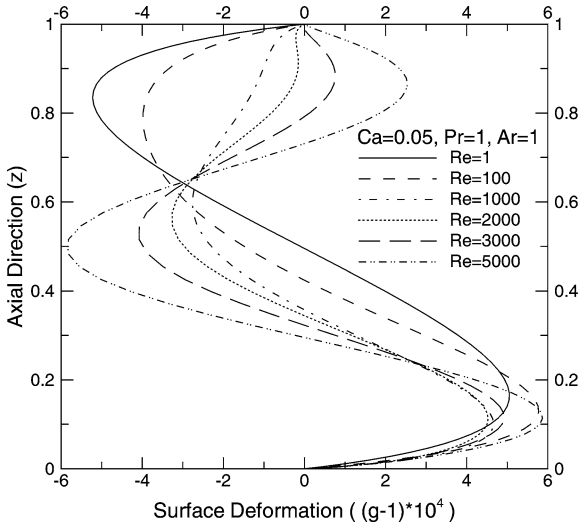

Fig. 2. Steady, axisymmetric free surface deformations with $Bi = 0$, $Ca = 0.05$ and various Re. There are two peaks of the free surface at low Re, while three peaks develops at $Re > 2000$.

Fig. 2. Déformation stationnaire axisymétrique de la surface libre pour $Bi = 0$, $Ca = 0{,}05$ et différents Re. Deux pics se développent sur la surface libre pour Re faible, et trois pour $Re > 2000$.

geometries [29,35]. While oscillatory thermocapillary convection in a rectangular cavity can be investigated in two-dimensional simulations [36], it cannot be realized in an open cylinder with a uniform heat flux [29] or in a liquid bridge. Oscillatory buoyant-thermocapillary convection was reported in axisymmetric simulations by Shevtsova and Legros [25], but no oscillations of pure thermocapillary convection was found in their axisymmetric simulations.

Fig. 2 shows two-dimensional free surfaces with $Pr = 1$, $Ar = 1$, $Bi = 0$, $Ca = 0.05$ and various Re. The free surfaces are convex near the lower cold wall, and change from concave to convex with increasing Re near the hot wall because of stronger returned-flow in the interior. At sufficiently low Re, the free surface is almost asymmetric about its mid point. It has two peaks and is elevated near the cold stagnation point where surface pressure achieves its maximum value. As Re increases at fixed Ca, the free surface develops three peeks. The surface deformation is $O(10^{-4})$, and its maximum value is 1.2×10^{-3} with $Ca = 0.1$.

Curvature of the free surface, sign and magnitude, is determined by both the surface pressure and normal viscous stresses as shown in Eq. (17). The curvature of the free surface is always negative near the cold corner where pressure is positive and large. Near the hot corner, the curvature changes from positive to negative with increasing Re even though surface pressure is always negative there. Thus, the change of curvature near the hot corner with increasing Re is induced by the normal viscous stresses. At $Re = 1$, normal viscous stresses are small, and the surface deformation shown in Fig. 2 correlates with surface pressure variation. With increasing Re, the influence of normal viscous stresses increases and together with the pressure they determine the shape of the interface. Evidently, surface elevation near the hot corner at the largest Re is driven by the normal viscous stresses.

Surface elevations and depressions increase with increasing Ca, while its shape is independent of Ca at a fixed Re. Stream function minima, surface temperatures and velocities with various Ca at a fixed Re are almost independent of Ca [33]. Thus dynamic free-surface deformations with $Ca \leqslant 0.1$ do not influence the convection in the liquid bridge. More details on the axisymmetric results appear in [30,31,33].

2.3. Three-dimensional thermocapillary convection with nondeformable surfaces

With $Ar = 0.714$, $Pr = 27$, Re_c for onset of oscillations with $V = 1.138$ (convex), 1 (flat) and 0.755 (concave) are about 210, 210 and 220, respectively. Fig. 3 shows temperature fluctuations in the section $z = 0.53$ and at the free surface at these values of V. The temperature fluctuations with $V \geqslant 1$ consist of a hot and a cold spot rotating clockwise, i.e., $m = 1$. This rotating pattern with $m = 1$ remains unchanged with increasing Re. Two pairs of hot and cold spots, i.e., a wavenumber of 2, are rotating clockwise with $V < 1$.

Fig. 4 shows the variation of Re_c and m with V at various Bi. Heat loss from the free surface stabilizes the flow as it tends to decrease the free surface temperature gradient, and Re_c increases with increasing Bi. With $Bi = 0$, a pair of wavenumbers are observed, and a transition from $m = 1$ to $m = 2$ occurs at V of about 0.9. The wavenumber can change with Bi. This change in wavenumber was reported in experiments [13], where a wavenumber of 1 was changed into 2 by altering the surrounding conditions of a liquid bridge.

Heat loss to surroundings is through forced convection induced by the free surface flow. The value of h for gases in forced convection is in the range 25−250 W/(m^2 K). With $H = 1.4$ mm in experiments [12], Bi is in the range 0.32–3.2. In the three-dimensional numerical simulations with a flat surface and $Pr = 7$ of [26], Bi of 6.4 was necessary to compare with the experimental results of [4]. Thus, our $Bi = 1$ (a much smaller bridge) is a reasonable assumption to compare with the experimental results of [12]. In addition, our previous work [2,35,37] showed that the inclusion of surface heat loss was necessary to achieve better agreement with experiments. When our numerical results with $Bi = 1$ are compared with those from normal gravity experiments [12], the wavenumber of 1 and the rotating mode are in good agreement. With $V = 1$, transition to $m = 1$ from $m = 2$ occurs at $Bi = 0.5$. Re_c is about 400 and $m = 1$ with $V = 1$ and $Bi = 0.5$. With $Bi > 0$, two different branches can exist in the stability diagram ($Re_c - V$). The most stable range of V with $Bi = 1$ is near 0.94 which is not in good agreement with experimental result [12], $V = 0.87$. However, in the experiments by Sumner et al. [14] at a higher Pr, the most stable range was near $V = 0.95$. Other experiments [13] showed that the range was very close to $V = 1$. Although the experiments

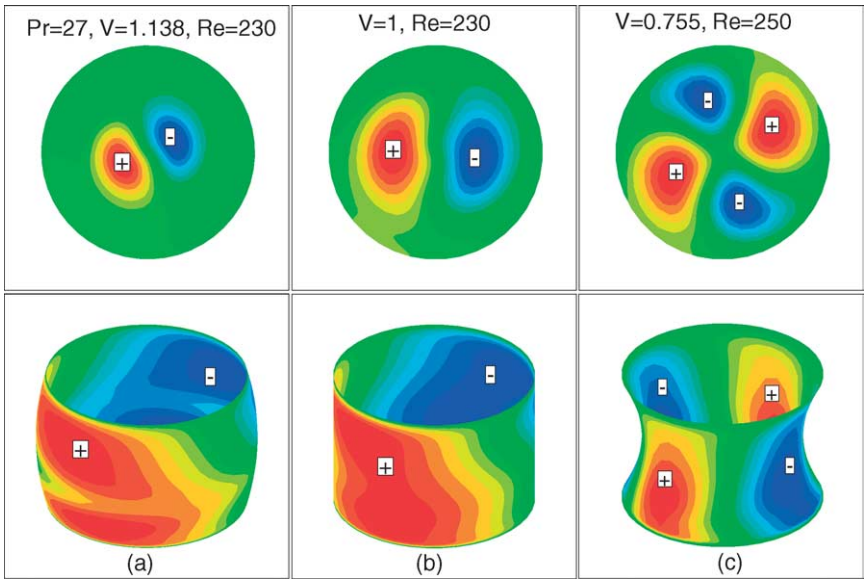

Fig. 3. Snapshots of temperature fluctuations in the section ($z = 0.53$) and the free surface with $Bi = 0$, $Ar = 0.714$ and various V. One or two pairs of hot and cold spots are observed.

Fig. 3. Fluctuations de température dans la section ($z = 0{,}53$) et à la surface libre pour $Bi = 0$, $Ar = 0{,}714$ et différents V. Une ou deux paires de points chaud et froid sont observées.

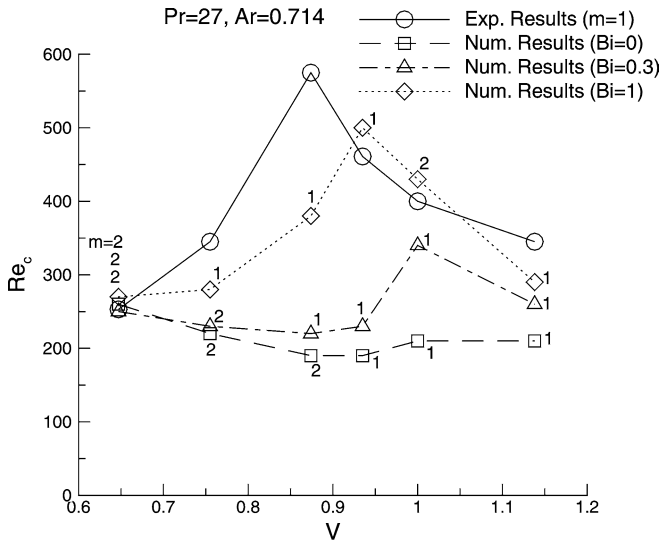

Fig. 4. Variations of Re_c and m with Bi where the experimental results are from [12]. Two different branches are observed in the stability diagram with $Bi > 0$.

Fig. 4. Variations de Re_c et m avec Bi, résultats expérimentaux d'après la référence [12]. Deux branches sont observées sur le diagramme de stabilité pour $Bi > 0$.

were performed with small rods, the difference between numerical and experimental results may be due to gravity-induced bridge deformation since the largest static Bond number ($Bd = \rho g H^2/\sigma$) in the experiments [12] was 2.

3. Thermocapillary convection in an open cylindrical annulus

Schwabe et al. [38] studied experimentally thermocapillary flows with $Pr = 17$ in two types of shallow liquid layers heated from the side: one is a rectangular configuration, the other an annular slot. In the annular slot heated from the inner rod, they observed azimuthal wavetrains travelling on the free surface, and found that the number of wavetrains increased as Ma increased. Kamotani et al. [39] investigated experimentally surface tension driven convection with 2 cSt silicone oils induced by placing a cylindrical heater at the center of annuli. Their experiments included flat and curved surfaces, which were determined by the liquid volume. Three-dimensional simulations of thermocapillary convection in an open cylindrical annulus heated from the inside wall were first reported by Sim and Zebib [37]. Four kinds of isotherm patterns at the free surface were observed with increasing Re: a two- and a three-lobed clockwise rotating pattern, and a two- and a three-lobed pulsating pattern. They found that heat loss from the free surface provided a satisfactory explanation for the Ma_c dependence on the container size at fixed aspect ratio which was observed in the experiments [39].

3.1. Mathematical model

The physical system considered is that in the microgravity experiment MAGIA [2] and is shown in Fig. 1(b). It is a cylindrical annulus with inner and outer radii, Ri and Ro, which is filled with an incompressible, $Pr = 6.84$ Newtonian fluid to a height H. The aspect ratio, Ar, is defined as $(Ro - Ri)/H$, and the values of Ar considered are 1, 2.5, 3.33, and 8 (which correspond to different values of H with Ri and Ro fixed at $Ri/Ro = 0.5$). The vertical inside and outside walls have cold and hot temperatures, $Ti = T_{\text{cold}}$ and $To = T_{\text{hot}}$, respectively. The bottom is an

adiabatic solid wall. The horizontal free surface is assumed nondeformable and has convective heat loss to the surroundings with the ambient temperature, T_∞ ($= T_{\text{cold}}$).

The nondimensional governing equations are Eqs. (2)–(4). Re, Pr, Ma and scales for nomalization are the same as those from the previous section. The boundary conditions become

$$\frac{\partial u}{\partial z} + \frac{\partial T}{\partial r} = 0, \quad v = 0, \quad \frac{\partial w}{\partial z} + \frac{1}{r}\frac{\partial T}{\partial \theta} = 0, \quad \frac{\partial T}{\partial z} = -Bi\,T, \quad \text{at } z = 1 \tag{20}$$

$$u = 0, \quad v = 0, \quad w = 0, \quad \frac{\partial T}{\partial z} = 0, \quad \text{at } z = 0 \tag{21}$$

$$u = 0, \quad v = 0, \quad w = 0, \quad T = 0, \quad \text{at } r = Ri/H \tag{22}$$

$$u = 0, \quad v = 0, \quad w = 0, \quad T = 1, \quad \text{at } r = Ro/H \tag{23}$$

3.2. Three-dimensional thermocapillary convection with flat surfaces

Re_c for onset of oscillations with $Bi = 0$, $Pr = 6.84$ and Ar = 1, 2.5, 3.33 and 8 are about 740, 490, 490 and 560, respectively. At Re_c, the flow is steady and the isotherms on the free surface are just circular lines, i.e. axisymmetric. Fig. 5 shows instantaneous temperature distributions on the free surface with various Ar. At $Ar = 1$, five azimuthal waves are rotating clockwise in agreement with similar finding in the experiments [2], and the pattern of five azimuthal waves remains unchanged with increasing Re. The isotherms have the same shape when rotated by $2\pi/5$. Thus if one measures the temperature at a fixed point on the free surface, the frequency of the temperature oscillations will be five times the isotherm rotation frequency. This is in agreement with the experimental results for the annular gap by Kamotani et al. [39], but with two azimuthal rotating waves (with $Ar < 1$).

While nine azimuthal waves near the critical region appear on the free surface with $Ar = 2.5$, ten azimuthal waves are observed at $Re = 800$ [35]. This is in reasonable agreement with the results from the experiments [2], where 11 azimuthal waves are observed at $Re = 2.5Re_c$. With $Ar = 3.33$, the twelve azimuthal waves are rotating clockwise near the critical region [35]. It is evident that the number of azimuthal rotating waves near the critical region increases with increasing Ar.

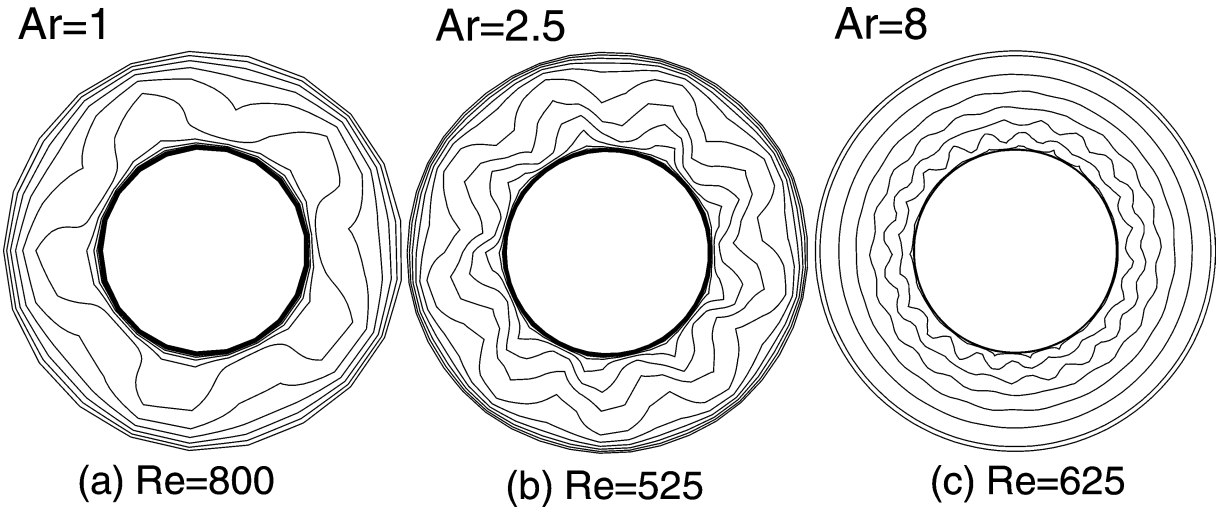

Fig. 5. Surface temperature distribution with $Bi = 0$ and: (a) $Ar = 1$ and $Re = 800$; (b) $Ar = 2.5$ and $Re = 525$; (c) $Ar = 8$ and $Re = 625$.

Fig. 5. Distribution de la température à la surface pour $Bi = 0$ et : (a) $Ar = 1$ et $Re = 800$; (b) $Ar = 2{,}5$ et $Re = 525$; (c) $Ar = 8$ et $Re = 625$.

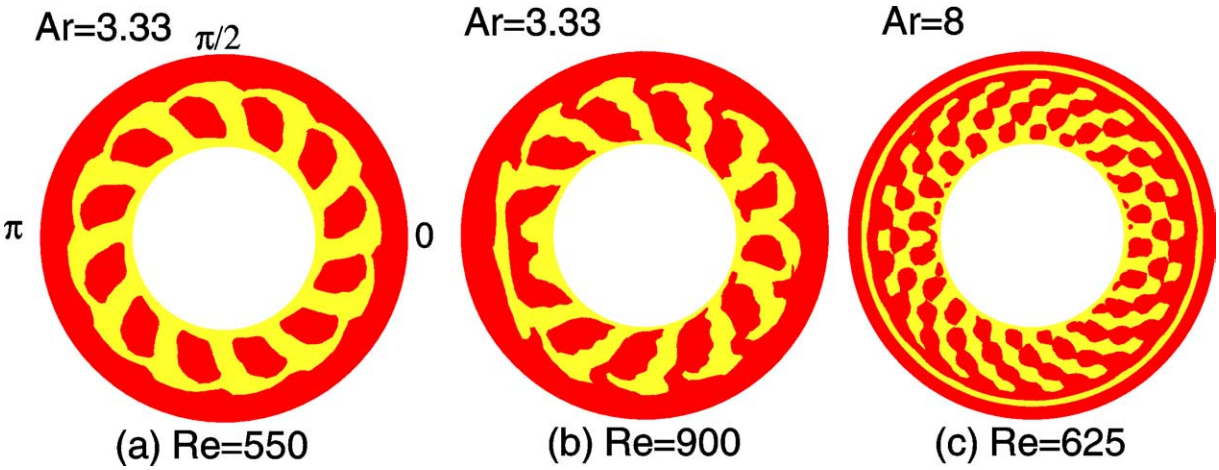

Fig. 6. Shadowgraphic snapshots (contours of $\nabla^2 T$) at the free surface with $Bi = 0$ and: (a) $Ar = 3.33$ and $Re = 550$; (b) $Ar = 3.33$ and $Re = 900$; and (c) $Ar = 8$ and $Re = 625$. (a) Shows azimuthal clockwise rotating waves, while (b) indicates azimuthal waves with a source and sink near respectively $\theta = \pi$ and 0. (c) Shows azimuthal standing waves with a source and sink near respectively $\theta = 0$ and π.

Fig. 6. Contours du laplacien de température ($\nabla^2 T$) à la surface libre pour $Bi = 0$ et : (a) $Ar = 3{,}33$ et $Re = 550$; (b) $Ar = 3{,}33$ et $Re = 900$; et (c) $Ar = 8$ et $Re = 625$. (a) Ondes azimutales rotatives (sens des aiguilles d'une montre), (b) ondes azimutales rotatives avec source et puits proches de $\theta = \pi$ et 0 respectivement. (c) Ondes azimutales rotatives avec source et puits proches de $\theta = 0$ et π respectivement.

Twenty azimuthal wavetrains with $Ar = 8$ are found on the free surface, and the waves are pulsating [35]. The inside wall looks like the source of the waves: the waves are generated at the inside cold wall and travel to the outside hot wall. This is in good agreement with the hydrothermal waves in the infinite layer model [15] and the rectangular cavity simulations [36]. We thus have travelling r-waves and pulsating θ-waves in cylindrical-shallow liquid layers. As Re increases these waves propagate far from the inside wall. The critical wavelength $\lambda = 2.5$ ($Pr = 6.84$) from linear theory [15] implies a wave number of 20 at the inside wall, which is in good agreement with our numerical result.

Fig. 6 shows shadowgraphic snapshots at the free surface with $Ar = 3.33$ and 8. Because the waves travel from the inside to the outside wall and rotate azimuthally clockwise near Re_c with $Ar = 3.33$, a supercritical spiral structure appears on the free surface as shown in Fig. 6(a). At higher Re with $Ar = 3.33$, the source and sink at the free surface are observed near $\theta = \pi$ and 0, respectively. A pattern with travelling r-waves and source-sink θ-waves, which propagate from a source into opposite directions to a sink, is shown in Fig. 6(b). However, with $Ar = 8$ slightly supercritical convection is in the form of travelling r-waves and pulsating source-sink θ-waves. These kinds of spiral patterns are in agreement with experimental results [40].

In steady state, only single-roll flow structure in a meridional section is available with $Ar = 1$, 2.5, 3.33 and 8. However, just above critical, two and three rolls are observed with $Ar = 3.33$ and 8, respectively [35]. Three rolls at $Ar = 8$ is in perfect agreement with space experiment [2]. The number of rolls increases with increasing Ar. We can expect the multi-roll structure to appear beyond Re_c in the case of shallow liquid layers. The axisymmetric results are very different from those of two-dimensional rectangular cavities reported by Xu and Zebib [36], where a critical Ar exists, the multi-structure appears at subcritical Re, and the flow can be stable with multi-structure in restabilized region (highly supercritical Re). However, the structures of three-dimensional states in shallow cylindrical and rectangular cavities have in common travelling multi-cells from the cold to hot corners with a standing, pulsating pattern in the third direction.

Fig. 7 shows the effect of Bi on Re_c and the critical dimensional-period, τ_c. The numerical results with $Bi = 0$ are in good qualitative but not in good quantitative agreement with the experiments [2]. The value of h is 25 to 250 W/(m^2 K) for gases in forced convection. Because of evaporation, the value will be increased substantially. It

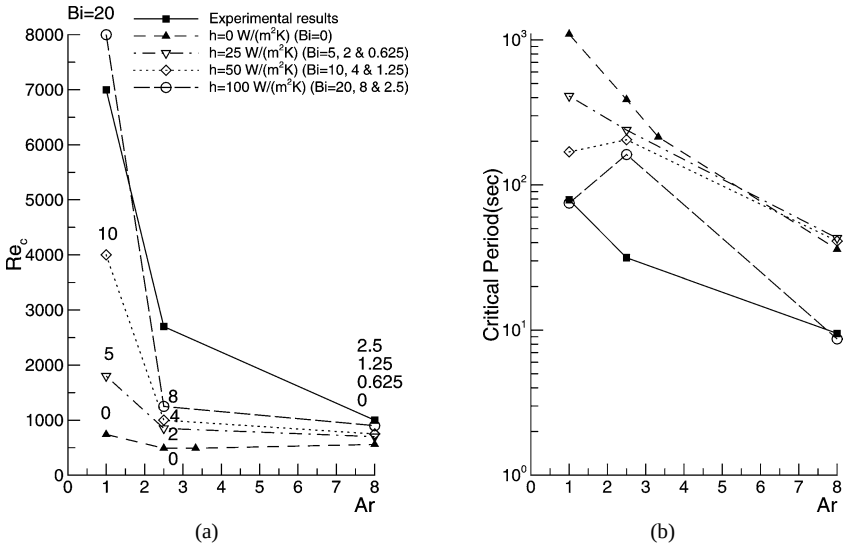

Fig. 7. Re_c and τ_c corresponding to various Ar at various Bi cooling the free surface. Heat loss from the free surface stabilizes the flow, and Re_c increases with increasing Bi at fixed Ar. τ_c decreases with Ar (Bi) at fixed Bi (Ar). Note that the curves here are for constant h so that Bi decreases along these curves with increasing Ar.

Fig. 7. Re_c et τ_c pour différents Ar et Bi de refroidissement à la surface libre. Les pertes de chaleur à la surface libre stabilisent l'écoulement et Re_c croît avec Bi pour Ar fixé. τ_c décroît avec $Ar(Bi)$ à Bi fixé. Les courbes sont tracées à h constant et Bi décroît le long de ces courbes lorsque Ar croît.

can be seen that heat loss from the free surface stabilizes the flow, and Re_c increases with increasing Bi. τ_c decreases with increasing Bi. It is observed that better comparison with experiments is achieved at the larger values of Bi.

In the experiments [2], it is argued that the free surface is effectively heated by the surroundings. Numerical results [35] with heating from surroundings approach the experimental results [2] with increasing Bi with good agreement obtained at $Bi = 0.5$.

3.3. Dynamic axisymmetric free-surface deformations

The physical system is an open cylindrical annulus with inner and outer radii, $Ri = 0.1Ro$ and Ro, heated from the inside wall. The deformable free surface is obtained as a solution of the coupled transport equations, assuming pinned contact points. The mathematical and numerical models can be found in [41].

Thermocapillary convection up to $Re = 5000$ with $Pr = 30,\ Ar = 1, Bi = 0$ and $Ca \leqslant 0.1$ was computed and no axisymmetric oscillatory states with either nondeformable or deformable surfaces were found. In three-dimensional numerical simulations with $Pr = 30,\ Ar = 1,\ Bi = 0$ and $Ca = 0$ (nondeformable flat surface), the critical Reynolds was about 2200 [37]. Thus dynamic free-surface deformations do not induce transition to unsteady, oscillatory axisymmetric convection, and only azimuthal waves can generate oscillations in this model. Thus we may conclude that time-dependent, large Pr thermocapillary convection with the wavenumber of 0 does not occur in cylindrical geometries near $Ar = 1$ [29,33,35].

Fig. 8 shows free surfaces with $Ca = 0.05$ and various Re. The surface is convex near the cold wall where surface pressure has a maximum positive value at the stagnation point, and concave near the hot wall. Two peaks appear at the free surface at sufficiently low Re and its curvature is determined by surface pressure [41]. As Re increases, the effect of normal viscous stresses increases. Additional ripples occur at the free surface which can be convex close to the hot corner. Surface elevations and depressions decrease with increasing Re due to this change in topology, volume conservation and curvature.

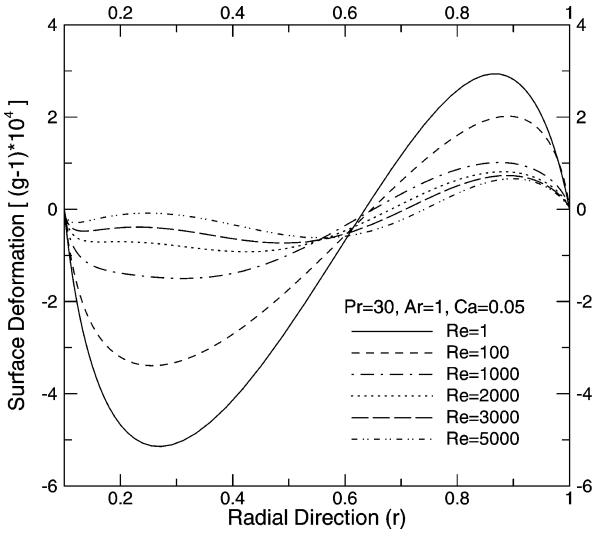

Fig. 8. Free surface deformations with $V = 1,\ Bi = 0,\ Ca = 0.05$ and various *Re*. Two free surface peaks increase to four with increasing *Re*.

Fig. 8. Déformation de la surface libre pour $V = 1,\ Bi = 0,\ Ca = 0{,}05$ et différents *Re*. On observe le passage de deux pics de surface à quatre lorsqu'on accroît *Re*.

The shape of the surface, number of ripples, and reflection point do not change with *Ca* at a fixed *Re*, while the magnitudes of depressions and elevations increase with increasing *Ca*. Surface deformation is $O(10^{-4})$. Its maximum value is 1.2×10^{-3}, about 0.12% of the cylinder height, with $Re = 1$ and $Ca = 0.1$. Stream function minima, and surface temperature and velocity distributions are independent of *Ca*. Thus, dynamic surface deformations with $Ca \leqslant 0.1$ have little effect on the convection. This result is consistent with that from liquid bridges [33].

4. Conclusion

Thermocapillary convection in liquid bridges and open cylindrical annuli is investigated in two- and three-dimensional numerical studies. Convection is steady and axisymmetric at sufficiently low values of *Re*, with either nondeformable or deformable surfaces. For the parameter ranges considered, it is found that dynamic free-surface deformations do not induce transitions to oscillatory convection in axisymmetric models and only steady convection is possible at any *Re* in strictly axisymmetric computations with either nondeformable or deformable surfaces. Transition to oscillatory three-dimensional motions occurs as *Re* increases beyond a critical value dependent on the aspect ratio, the Prandtl number and the fluid volume.

Acknowledgements

This work was supported by the Brain Korea 21 Project in 2003. We gratefully acknowledge the support of BK 21 and computer resources from the Rutgers Computational Grid composed of a Distributed Linux PC Cluster on which all computations were performed.

References

[1] D. Schwabe, Marangoni effects in crystal growth melts, Phys. Chem. Hydrodynam. 2 (1981) 263–280.
[2] D. Schwabe, A. Zebib, B.-C. Sim, Oscillatory thermocapillary convection in open cylindrical annuli. Part 1. Experiments under microgravity, J. Fluid Mech. 491 (2003) 239–258.
[3] P. Rudolph, Fundamental studies on bridgman growth of CdTe, Prog. Crystal Growth and Charact. 29 (1994) 275–381.
[4] F. Preisser, D. Schwabe, A. Scharmann, Steady and oscillatory thermocapillary convection in liquid columns with free cylindrical surface, J. Fluid Mech. 126 (1983) 545–567.
[5] R. Velten, D. Schwabe, A. Scharmann, The periodic instability of thermocapillary convection in cylindrical liquid bridges, Phys. Fluids 3 (1991) 267–279.
[6] L. Carotenuto, D. Castagnolo, C. Albanese, R. Monti, Instability of thermocapillary convection in liquid bridges, Phys. Fluids 10 (1998) 555–565.
[7] R. Monti, R. Savino, M. Lappa, Flight results on Marangoni flow instability in liquid bridges, Acta Astonautica 47 (2000) 325–334.
[8] K. Muehlner, M. Schatz, V. Petrov, W. McCormick, J. Swift, H. Swinney, Observation of helical traveling-wave convection in a liquid bridge, Phys. Fluids 9 (1997) 1850–1852.
[9] D. Schwabe, S. Frank, Experiments on the transition to chaotic thermocapillary flow in floating zones under microgravity, Adv. Space Res. 24 (1999) 1391–1396.
[10] D. Schwabe, R. Velten, The multi-roll-structure of thermocapillary flow and its transition to oscillatory flow in long floating zones with length L near the Rayleigh-limit and restationarization above the critical Marangoni number, J. Jpn Soc. Microgravity Appl. 15 (1998) 425–430.
[11] W. Hu, J. Shu, R. Zhou, Z. Tang, Influence of liquid bridge volume on the onset of oscillation in floating zone convection. I. Experiments, J. Cryst. Growth 142 (1994) 379–384.
[12] J. Masud, Y. Kamotani, S. Ostrach, Oscillatory thermocapillary flow in cylindrical columns of high Prandtl number fluids, J. Thermophys. Heat Transfer 11 (1997) 105–111.
[13] V. Shevtsova, M. Mojahed, J. Legros, The loss of stability in ground based experiments in liquid bridges, Acta Astronautica 44 (1999) 625–634.
[14] L. Sumner, G. Neitzel, J.-P. Fontaine, P. Dell'Aversana, Oscillatory thermocapillary convection in liquid bridges with highly deformed free surfaces: Experiments and energy-stability analysis, Phys. Fluids 13 (2001) 107–120.
[15] M. Smith, S. Davis, Instabilities of dynamic thermocapillary liquid layers: Part 1. Convective instabilities, J. Fluid Mech. 132 (1983) 119–144.
[16] J.-J. Xu, S. Davis, Convective thermocapillary instabilities in liquid bridges, Phys. Fluids 27 (1984) 1102–1107.
[17] H. Kuhlmann, H. Rath, Hydrodynamic instabilities in cylindrical thermocapillary liquid bridges, J. Fluid Mech. 247 (1993) 247–274.
[18] M. Levenstam, G. Amberg, Hydrodynamic instabilities of thermocapillary flow in a half-zone, J. Fluid Mech. 297 (1995) 357–372.
[19] M. Wanschura, V. Shevtsova, H. Kuhlmann, H. Rath, Convective instability mechanisms in thermocapillary liquid bridges, Phys. Fluids 7 (1995) 912–925.
[20] G. Neitzel, K.-T. Chang, D. Jankowski, H. Mittelmann, Linear-stability theory of thermocapillary convection in a model of the float-zone crystal-growth process, Phys. Fluids 5 (1993) 108–114.
[21] M. Levenstam, G. Amberg, C. Winkler, Instabilities of thermocapillary convection in a half-zone at intermediate Prandtl numbers, Phys. Fluids 13 (2001) 807–816.
[22] Q. Chen, W. Hu, Influence of liquid bridge volume on instability of floating half zone convection, Int. J. Heat Mass Transfer 41 (1998) 825–837.
[23] Y. Tao, R. Sakidja, S. Kou, Computer simulation and flow visualization of thermocapillary flow in a silicone oil floating zone, Int. J. Heat Mass Transfer 38 (1995) 503–510.
[24] R. Savino, R. Monti, Oscillatory Marangoni convection in cylindrical liquid bridges, Phys. Fluids 8 (1996) 2906–2922.
[25] V. Shevtsova, J. Legros, Oscillatory convective motion in deformed liquid bridges, Phys. Fluids 10 (1998) 1621–1634.
[26] J. Leypoldt, H. Kuhlmann, H. Rath, Three-dimensional numerical simulation of thermocapillary flows in cylindrical liquid bridges, J. Fluid Mech. 414 (2000) 285–314.
[27] V. Shevtsova, D. Melnikov, J. Legros, Three-dimensional simulations of hydrodynamic instability in liquid bridges: influence of temperature-dependent viscosity, Phys. Fluids 13 (2001) 2851–2865.
[28] M. Lappa, R. Savino, R. Monti, Three-dimensional numerical simulation of Marangoni instabilities in non-cylindrical liquid bridges in microgravity, Int. J. Heat Mass Transfer 44 (2001) 1983–2003.
[29] B.-C. Sim, A. Zebib, Thermocapillary convection in open cylinders with undeformable curved surfaces, Int. J. Heat Mass Transfer 45 (2002) 4983–4994.
[30] B.-C. Sim, A. Zebib, Thermocapillary convection in liquid bridges with undeformable curved surfaces, J. Thermophys. Heat Transfer 16 (2002) 553–561.
[31] B.-C. Sim, Thermocapillary convection in cylindrical geometries, Ph.D. dissertation, Rutgers University, 2002.
[32] M. Mundrane, A. Zebib, Low Prandtl number Marangoni convetion with a deformable interface, J. Thermophys. Heat Transfer 9 (1995) 795–797.

[33] B.-C. Sim, W.-S. Kim, A. Zebib, Dynamic free-surface deformations in axisymmetric liquid bridges, Adv. Space Res. (2003), submitted for publication.
[34] H. Kuhlman, C. Nienhuser, Dynamic free-surface deformations in thermocapillary liquid bridges, Fluid Dynamics Res. 31 (2002) 103–127.
[35] B.-C. Sim, A. Zebib, D. Schwabe, Oscillatory thermocapillary convection in open cylindrical annuli. Part 2. Simulations, J. Fluid Mech. 491 (2003) 259–274.
[36] J. Xu, A. Zebib, Oscillatory two- and three-dimensional thermocapillary convection, J. Fluid Mech. 364 (1998) 187–209.
[37] B.-C. Sim, A. Zebib, Effect of surface heat loss and rotation on transition to oscillatory thermocapillary convection, Phys. Fluids 14 (2002) 225–231.
[38] D. Schwabe, U. Moller, J. Schneider, A. Scharmann, Instabilities of shallow dynamic thermocapillary liquid layers, Phys. Fluids 4 (1992) 2368–2381.
[39] Y. Kamotani, S. Ostrach, J. Masud, Microgravity experiments and analysis of oscillatory thermocapillary flows in cylindrical containers, J. Fluid Mech. 410 (2000) 211–233.
[40] N. Garnier, A. Chiffaudel, Two dimensional hydrothermal waves in an extended cylindrical vessel, Eur. Phys. J. B 19 (2001) 87–95.
[41] B.-C. Sim, W.-S. Kim, A. Zebib, Axisymmetric thermocapillary convection in open cylindrical annuli with deforming interfaces, Int. J. Heat Mass Transfer (2003), submitted for publication.